Metastable Metal Ion Production in Sputtering dc Glow Discharge Plasmas: Characterization by Electronic State Chromatography

William S. Taylor,* Eddie M. Spicer, and Daniel F. Barnas

Department of Chemistry, University of Central Arkansas, Conway, Arkansas 72035

Received: September 29, 1998; In Final Form: December 1, 1998

The sputtering dc glow discharge is a stable and intense source of a wide variety of metal ions for use in ion/molecule studies. We have examined factors influencing the formation of metastable excited states of sputtered species in this device using the electronic state chromatography (ESC) technique. These determinations are essential if the glow discharge is to be used as a source of metal ions for subsequent reaction, since the electronic configuration of the metal can dramatically affect its reactivity in the gas phase. Further, the ability to manipulate excited-state production provides the means for the study of state-specific behavior of these species. We have obtained evidence in a series of experiments that indicates that the glow discharge is capable of producing several metal ions in metastable excited states as well as the ground state. Identification of specific configurations for several first-, second-, and third-row metal ions has been made on the basis of reduced zero-field mobilities in He. Results suggest that significant population of excited states higher than approximately 3.4 eV above the ion ground state does not occur in an Ar discharge for the metals examined here. Examination of the dependence of configuration distributions for several metal ions has revealed that excited-state production is sensitive to certain discharge parameters including pressure, distance to sampling orifice, and working gas composition. These results suggest that production of excited metal ions in the discharge involves energetic electrons. Further, some degree of deactivation of excited states occurs prior to extraction for ions whose excited states are collisionally coupled to lower states via interaction with the discharge gas. Metastable deactivation is enhanced in the third-row ions as a result of large spin−orbit effects.

Introduction

The utility of the sputtering glow discharge for elemental analysis in both optical and mass spectrometric applications is well-recognized.[1] More recently, the glow discharge (GD) has also been employed as an ion source for use in the study of transition metal ion chemistry.[2−4] In this application, the GD offers the benefits of intense ion signals, along with excellent stability. Further, the GD is capable of producing a wide variety of metal ions for subsequent reaction. These advantages make the GD an attractive alternative to other metal ion production methods, such as surface ionization and electron impact, which can suffer from low ion currents or are not as versatile in terms of the number of different metal ions that can be formed. One feature that the GD shares with several of these other ionization techniques is that it is capable of producing metal ions in excited states. The presence of excited species can have a profound effect on the observed chemistry of the metal ion, since the specific reactivity exhibited by the ion can be strongly influenced by its electronic configuration.[5−7] This is apparent in comparisons of the reactions of metal ions within a transition series, as well as those of a given metal ion in different electronic states. Although the state specificity of metal ion−molecule reactions has yielded a wealth of information regarding the electronic requirements for access to specific product channels, it can also complicate product analysis if the state distribution of the reactant ions is unknown at the time of the reaction. For this reason, studies of transition metal ion chemistry are usually accompanied by some attempt to determine the degree to which excited states are populated in the ionization step.

Here, we examine the excited-state production for several transition metal ions produced in the GD. Even though many excited metal ion states are energetically accessible within the discharge plasma, many of these are rapidly depopulated by optical emission. Thus, these states need not be considered in reactions carried out external to the discharge. More significant with regard to ion chemistry is the production of metastable excited states sufficiently long-lived to influence reactivity after extraction from the discharge. For the transition metals, these are states for which radiative relaxation to the ground state is spin- and/or parity-forbidden. This work also addresses the degree to which excited-state populations can be controlled by manipulation of various discharge parameters, demonstrating the effectiveness of the GD in studies of state-specific processes.

Experimental Section

Experiments were carried out using a drift cell apparatus, which has been described in detail previously.[2] Briefly, this instrument incorporates a sputtering dc glow discharge ion source to produce metal ions that are then directed to a 4.0 cm drift cell containing 3−5 Torr of He. Temperature control of the drift cell is accomplished via a copper jacket through which heated or cooled gases can be circulated. Temperatures within the drift cell are monitored using a thin-film platinum thermometer. Ions are drawn through the drift cell via a weak electric field. In this work, the field strength was adjusted such that E/N ranged from 2.2 to 8.9 Td. Ions exiting the drift cell are mass-analyzed via a quadrupole mass filter and subsequently detected using an electron multiplier. The output of the electron

10.1021/jp983887i CCC: $18.00
Published on Web 01/20/1999

multiplier is then sent to a multichannel scaler and the data can then be displayed in a number of formats on a laboratory computer. Typical metal ion signals measured after mass filtering under these conditions are in the range of 10^3-10^4 cps.

In this work, specific configurations of several metal ions produced in the GD were identified within the drift cell using a technique called electronic state chromatography (ESC),[8] which characterizes them on the basis of the their mobilities in He. ESC is most effective in distinguishing between electronic configurations that differ significantly in size, such as those that differ by the presence or absence of an s electron. The larger size of the s orbital results in a greater repulsive interaction between the ion and the He bath gas, which reduces the number of capture collisions. In terms of the first-row ions, this means that ions with $3d^{n-1}4s^1$ configurations have higher mobilities in the bath gas than those with $3d^n$ configurations. As a consequence, a pulse containing a given metal ion in both configurations will be separated within the drift cell such that the higher mobility configuration arrives at the detector first. Thus, configurations of sufficiently different mobilities appear as different peaks in an arrival time distribution (ATD). Ion mobilities used in assigning configurations were obtained from the ATD's by measuring the flight time of the different configurations as a function of the reciprocal of the drift voltage.[8] These were then normalized to 0 °C and 760 Torr and reported as reduced zero-field mobilities, K_0.

The purities of the sputter targets used were as follows: V, 99.7%; Cr, 99.5%; Co, 99.8%; Ni, 99.9%; Zn, 99.9%; Pd, 99.9%; Hf, 99.7%; Ta, 99.96%; W, 99.9995%; Re, 99.97%; Ir, 99.8%; Pt, 99.95%; Au, 99.9985%. The purities of Fe, Ag, and Cu were not known; however, mass spectra collected using these sputter targets revealed no discernible contaminants. V, Fe, Ni, Cu, Zn, Pd, Hf, Ta, W, Re, Ir, Pt, and Au were all obtained in rod or wire formats. The remaining metals were obtained as powders and pressed into pellets prior to sputtering. Argon and neon used as discharge gases had purities of 99.999% and 99.9995%, respectively. Helium was used in both the drift cell and the discharge with a purity of 99.9999%.

Results and Discussion

ESC analyses of several first-, second-, and third-row transition metal ions were carried out using Ar, Ne, and He discharges. Reduced zero-field mobilities measured in helium are summarized in Table 1, along with the available literature values and configuration assignments, which were made on the basis of the K_0 values.[8,9] Agreement between our K_0 values and those reported previously for specific configurations is excellent. ATD's of metal ions extracted from the discharge clearly indicate the presence of two configurations with significantly different mobilities for V^+, Cr^+, Fe^+, Co^+, Ni^+, Cu^+, Pd^+, Pt^+, and Au^+. The ATD for Co^+ is given in Figure 1. The relative intensities of the two configurations shown in this ATD are typical of what is observed for Co^+ when sampling from a ~1 Torr Ar discharge at a point well-removed (≥10 mm) from the cathode. Under the same discharge conditions, the configuration ratio for V^+ was comparable to that of Co^+, whereas the ATD's for the remaining ions listed above indicated excited-state configurations in lesser amounts relative to the ground state. However, as we will show, configuration ratios often exhibited significant variability with respect to discharge parameters. Pd^+, Pt^+, and Au^+ are notable in this regard in that the excited-state configurations were not observed at all unless specific discharge conditions existed.

Because several states may have the same configuration, the ATD's for these ions may be indicative of more than two states.

TABLE 1: Reduced Zero-Field Mobility Data for Selected First-, Second-, and Third-Row Transition Metal Ions

ion	configuration[a]	K_0 (this work)[b]	K_0 (lit.)[b,c]
V^+	**$3d^4$**	16 ± 1	16.7
	$3d^34s^1$	21.4 ± 0.2	22.0, 25.1[d]
Cr^+	**$3d^5$**	18.0 ± 0.3	17.5
	$3d^44s^1$		20.4, 21.4[d]
Fe^+	$3d^7$		16.9
	$3d^64s^1$	23 ± 1	23.7
Co^+	**$3d^8$**	15 ± 2	15.6
	$3d^74s^1$	22 ± 2	22.9
Ni^+	**$3d^9$**	16.2 ± 0.2	16.3
	$3d^84s^1$	24 ± 2	24.2
Cu^+	**$3d^{10}$**	15.8 ± 0.6	15.7
	$3d^94s^1$	22 ± 1	
Zn^+	**$3d^{10}4s^1$**	24 ± 2	23.4
Pd^+	**$4d^9$**	18.2 ± 0.6	
	$4d^85s^1$	23.2 ± 0.4	
Ag^+	**$4d^{10}$**	18 ± 1	
Hf^+	**$5d^16s^2$**	18 ± 1	
Ta^+	**$5d^36s^1$**	21 ± 1	
W^+	**$5d^46s^1$**	19.7 ± 0.9	
Re^+	**$5d^56s^1$**	19.4 ± 0.4	
Ir^+	**$5d^76s^1$**	20.2 ± 0.5	
Pt^+	**$5d^9$**	20.6 ± 0.9	
	$5d^86s^1$	23 ± 2	
Au^+	**$5d^{10}$**	19.5 ± 0.5	
	$5d^96s^1$	22 ± 2	
Hg^+	**$5d^{10}6d^1$**	19.1 ± 1	19.6[e]

[a] Ground-state configurations are indicated by boldface. [b] In units of $cm^2\ V^{-1}\ s^{-1}$. [c] Reference 8, unless otherwise specified. [d] More than one excited state observed. [e] Reference 9.

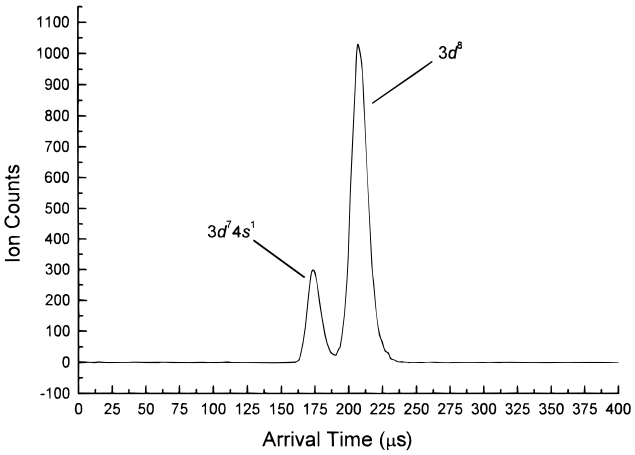

Figure 1. Arrival time distribution for Co^+ produced in an Ar discharge. $T = 303$ K; $E/N = 8.9$ Td.

Low-lying states for the first- and second-row ions examined here are listed in Table 2.[10] In some cases, high- and low-spin states of the same configuration have sufficiently different mobilities to be distinguished via ESC; however, this does not always occur. This was the case for our V^+ ATD's, where features attributable to several $3d^34s^1$ states reported by Kemper and Bowers were not observed.[8] If more than one state is present within the $3d^34s^1$ manifold for V^+ in our experiment, we are unable to resolve them. However, resolution for the V^+ ATD's was consistently poorer than that obtained for Cu^+ ATD's, despite the fact that the K_0 values for the two V^+ configurations are comparable to those of Cu^+. We believe that this is an indication that both high- and low-spin states of a given V^+ configuration are present and that the slight differences in their mobilities result in broadening of the peaks. Cr^+ ATD's contained a large fraction of a low-mobility feature consistent with the $3d^5$ configuration. A high-mobility feature was also observed for Cr^+ that we attribute to the $3d^44s^1$ configuration.

TABLE 2: Low-Lying Electronic States for Selected First- and Second-Row Transition Metal Ions[a]

ion	state	configuration	energy[b] (eV)	ion	state	configuration	energy[b] (eV)
V^+	a^5D	$3d^4$	0.026	**Co^+**	a^3F	$3d^8$	0.086
	a^5F	$3d^34s^1$	0.363		a^5F	$3d^74s^1$	0.515
	a^3F	$3d^34s^1$	1.104		b^3F	$3d^74s^1$	1.298
	a^3P	$3d^4$	1.452		a^3P	$3d^8$	1.655
	a^3H	$3d^4$	1.566		a^5P	$3d^74s^1$	2.228
	b^3F	$3d^4$	1.681		b^3P	$3d^74s^1$	2.998
	a^5P	$3d^34s^1$	1.692	**Ni^+**	a^2D	$3d^9$	0.075
	a^3G	$3d^4$	1.807		a^4F	$3d^84s^1$	1.160
	a^1G	$3d^34s^1$	2.370		a^2F	$3d^84s^1$	1.757
	b^3P	$3d^34s^1$	2.374		b^2D	$3d^84s^1$	2.899
	a^1I	$3d^4$	2.379	**Cu^+**	a^1S	$3d^{10}$	0.00
	a^1S	$3d^4$	2.468		a^3D	$3d^94s^1$	2.808
	c^3P	$3d^34s^1$	2.509		a^1D	$3d^94s^1$	3.257
Cr^+	a^6S	$3d^5$	0.000	Zn^+	^2S	$3d^{10}4s^1$	0.000
	a^6D	$3d^44s^1$	1.522		^2D	$3d^94s^2$	7.909
	a^4D	$3d^44s^1$	2.458	**Pd^+**	^2D	$4d^9$	0.219
	a^4G	$3d^5$	2.543		^4F	$4d^85s^1$	3.442
Fe^+	a^6D	$3d^64s^1$	0.052	Ag^+	^1S	$4d^{10}$	0.0
	a^4F	$3d^7$	0.300		^3D	$4d^95s^1$	5.110
	a^4D	$3d^64s^1$	1.032				
	a^4P	$3d^7$	1.688				
	a^2G	$3d^7$	1.993				

[a] Ions for which excited configurations were observed are in boldface. [b] Reference 10; averaged over *J*-levels.

In this case, however, the high-mobility feature could not be completely resolved at room temperature and no reliable K_0 value was obtained. Fe^+ ATD's were dominated by the single peak for which the mobility is reported. Here also, a feature was observed (this time at a longer arrival time than the main peak) that was incompletely resolved from the higher-mobility feature. We believe that this is a $3d^7$ excited state that is collisionally relaxed to a lower-energy state of higher mobility within the drift cell. This effect has been previously noted specifically with regard to the $a^6D(3d^64s^1)$ ground state and $a^4F(3d^7)$ first excited state of Fe^+ but can occur whenever a lower-energy state possesses a higher mobility than a higher-energy state.[8,11] Because the high-mobility state experiences a more repulsive interaction with He than the low-mobility configuration, the potential energy surfaces describing the interactions of the two Fe^+ configurations with He cross. This allows the low-mobility/high-energy configuration to be converted within the drift cell to the high-mobility/low-energy configuration. A similar process has been proposed previously for Sc^+ in which the ^3D ground state and the ^1D first excited state (both $3d^14s^1$) are coupled via the $^3F(3d^2)$ second excited state.[7] Configurations with different mobilities that are converted in this manner within the drift cell exhibit intermediate arrival times resulting in a bridging of the two peaks in the ATD. A similar explanation likely accounts for our inability to resolve the high-mobility feature in the Cr^+ ATD's and would suggest that the $a^4G(3d^5)$ state lying above the a^6D and a^4D states (both $3d^44s^1$) is being populated by the discharge. This seems reasonable given the minimal energy difference between the Cr^+ a^4D and a^4G states shown in Table 2. Finally, we note that in cases where such "configuration crossings" are possible, sufficient collisions with the discharge gas prior to extraction would result in some degree of relaxation of the excited configuration within the discharge itself, thus reducing the relative population of the higher energy configuration at the time of sampling. ATD's for Zn^+ and Ag^+ consist of only one peak, indicating that only one configuration (presumably the ground state) is present in the drift cell.

Upon examination of the specific cases in which excited states were observed, it is possible to establish approximate energetic limits on the excited states that are accessible in an Ar discharge under the conditions employed. Relative to the ion ground state, this upper limit falls within the range 3.442 eV $\leq E_{max} <$ 5.110 eV. The lower bound on this range corresponds to the ^4F first excited state of Pd^+, which is the lowest energy state to which the observed $4d^85s^1$ configuration can be assigned. The upper limit is the ^3D $(4d^95s^1)$ state of Ag^+, which is not observed. Potentially accessible states (those less than at least 3.442 eV) therefore include all of the low-lying states listed in Table 2 with the exceptions of $(^2D)Zn^+$ and $(^3D)Ag^+$. This is an additional indication that the different configurations observed in our ATD's are likely the result of several states. The approximate upper limit given above is useful in estimating which states are likely to be formed by the GD; however, metal ions within dc discharges are well-known to produce emissions from states higher in energy. The apparent energetic limit observed here simply illustrates that the state distribution, which is actually extracted from the GD, is influenced by both excitation and relaxation processes. In other words, the configurations that we observe via ESC may be populated by both promotion from lower states as well as deactivation of higher states and are themselves not rapidly depopulated within the discharge. Having said this, we again note that the amount of excited state present at the point of extraction is influenced by discharge conditions. We show below that the relative amount of excited configuration(s) sampled varies as a function of both the distance between the sampling orifice and the cathode as well as the pressure and identity of the discharge gas. Manipulation of these discharge parameters will affect either the availability of a necessary energetic precursor or the number and/or efficiency of relaxing collisions that the ions experience prior to extraction. Our observations suggest that in some cases, both effects contribute to the metal ion state distributions.

Spatial Effects. Figure 2 shows the high-mobility/low-mobility ratios for Cu^+ and Ni^+ with respect to the cathode position in both Ar and Ne discharges. For both ions, the relative amount of the high-mobility (excited) configuration is enhanced as metal ions are sampled closer to the cathode but drops to a constant value several millimeters from the cathode. Figure 3 shows absolute peak areas of the high-mobility and low-mobility configurations as a function of cathode position for Cu^+ in an Ar discharge. Examination of this figure illustrates again that production of excited Cu^+ reaches a maximum value closer to the cathode than the ground state. Further, production of both configurations falls dramatically within 2−3 mm of the cathode.

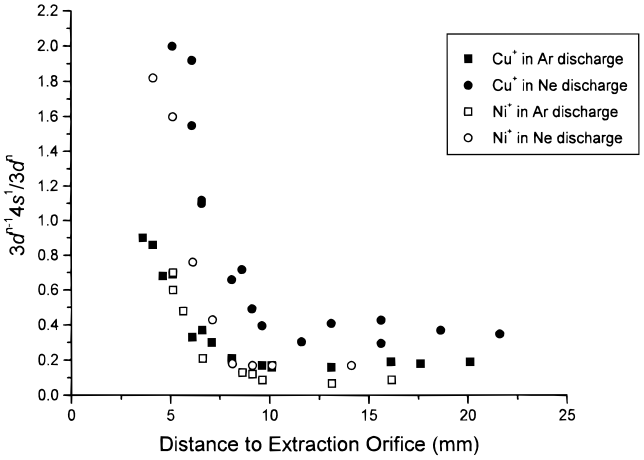

Figure 2. High-mobility/low-mobility configuration ratios as a function of distance to sampling orifice for Cu^+ and Ni^+ ions produced in Ar (1 Torr) and Ne (2 Torr) discharges. Discharge current = 6.25 mA (Cu^+, Ni^+ in Ar), 5.50 mA (Cu^+ in Ne), 8.00 mA (Ni^+ in Ne).

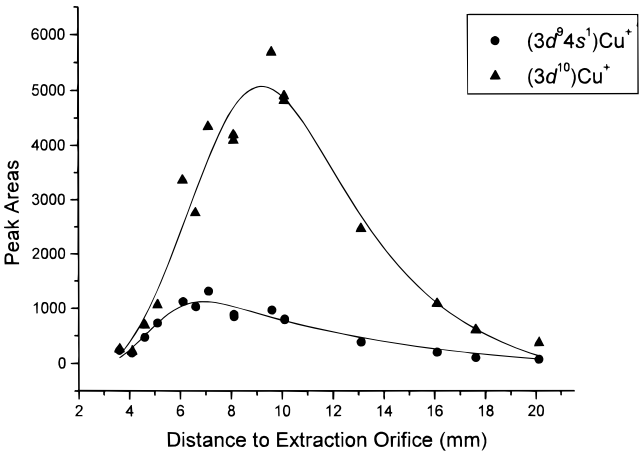

Figure 3. Cu^+ high-mobility and low-mobility peak areas as a function of distance to sampling orifice. Ions produced in Ar discharge; discharge current = 6.25 mA; discharge pressure = 1 Torr.

This drop in the sputtered ion signal indicates the onset of the transition zone between a region of large potential drop known as the cathode dark space (CDS) and the intensely luminous negative glow (NG). Any positive ion that is formed within or migrates into the CDS is subjected to a large field gradient and drawn to the cathode surface instead of being sampled.

Ionization of sputtered metal atoms within the discharge is thought to occur as a result of several possible mechanisms, including Penning ionization via metastables of the discharge gas, asymmetric charge transfer with ions of the discharge gas, and electron impact ionization. Of these, Penning ionization is generally believed to be the most significant within the NG under the discharge conditions employed here, although electron impact ionization is also thought to contribute to the formation of metal ions near the boundary between the CDS and the NG.[12,13] In this region, fast electrons enter the negative glow after being accelerated across the CDS. Electron energies reach a maximum at this boundary, and then decrease to an average constant value within a few millimeters of the cathode as a result of relaxing collisions within the NG. Further, the electron density is highest near the edge of the CDS.[14] Because metastable species of the discharge gas are also produced via collisions with fast electrons, the number density of these species is also high near the CDS/NG boundary.[15]

It is thought that Penning ionization becomes more probable the greater the energy difference between the resulting metal ion and electron and thus likely produces ions primarily in their ground states.[16] Our results suggest that the metastable metal ions are produced from processes involving energetic electrons. The observation that Cu^+ and Ni^+ high-mobility/low-mobility ratios increase nearer the cathode is consistent with the two configurations being formed by different mechanisms and that these mechanisms exhibit different spatial dependencies. This is also supported by the configurations that are observed for Pd^+ and Ag^+, two of the ions examined here with the highest energy first excited states. Simply on the basis of energetics, the $^4F_{9/2}$ and $^4F_{7/2}$ states of Pd^+ (both $4d^85s^1$) should be accessible from ground-state Pd atoms via the Ar metastables at 11.5 and 11.7 eV. Likewise, the Ne metastable states at 16.6 and 16.7 eV possess ample energy to produce numerous $Pd^+(4d^85s^1)$ states, as well as the ^3D and ^1D states of Ag^+ (both $4d^95s^1$). However, despite favorable energetics, no high-mobility configurations of Ag^+ are observed in either Ar or Ne discharges, and the $4d^85s^1$ configuration of Pd^+ is observed in small amounts only when the ions are sampled near the CDS/NG boundary. The spatial dependence of $Pd^+(4d^85s^1)$ indicates that an energetic precursor is required that is not present in the NG but becomes more abundant nearer to the cathode. Metastables of the discharge gas occur throughout the NG as well as in the CDS/NG region, while the electron energy distribution function (EEDF) becomes richer in high-energy electrons nearer the cathode. Thus, our Pd^+ observations argue against Penning ionization as the source of excited metal ions and are consistent with an electron impact ionization/excitation process involving energetic electrons. The 12.686 eV (ionization energy + excitation energy) necessary to populate the $^3D(4d^95s^1)$ first excited state of Ag^+ from ground-state Ag atoms would require an EEDF shifted to even higher energies, necessitating sampling even nearer the CDS/NG boundary in order to observe this excited configuration. The apparent absence of excited Ag^+ in Ar and Ne discharges could be an indication that these states are formed too close to the cathode fall to be sampled. Langmuir probe measurements within the NG region of Ar/Cu discharges operated under similar conditions to those employed here indicate EEDF's with maxima in the range of 1 eV.[17] Interestingly, these distributions are thought to indicate a depletion of high-energy electrons, which are presumably facilitating excitation processes such as the one described here. It has also been shown that the identity of the cathode material has little effect on the electron energy distribution, which is in agreement with our observation of similar energetic constraints on excited-state ion production regardless of the metal.[17]

Asymmetric charge transfer has also been implicated in the production of some excited metal ions in certain glow discharge applications.[16,18,19] This excitation mechanism is thought to be important only in discharge geometries where the current densities are much higher than those employed here; therefore, we do not consider this to be a significant contributor to the excited metal ion population in these experiments. This does, however, suggest that much higher internal energy distributions might be obtained for some ions with the use of hollow cathode or Grimm-type discharge geometries, both of which operate at higher plasma densities.

Pressure Effects. Figure 4 illustrates the effect of discharge pressure on the ratio of the high-mobility configuration to the low-mobility configuration for V^+, Co^+, Ni^+, and Cu^+. All ions were produced using Ar as the discharge gas under constant current conditions. Also, metal ions were extracted well away from the CDS/NG boundary. This was done in order to minimize any spatial influence on the high-mobility/low-mobility ratios

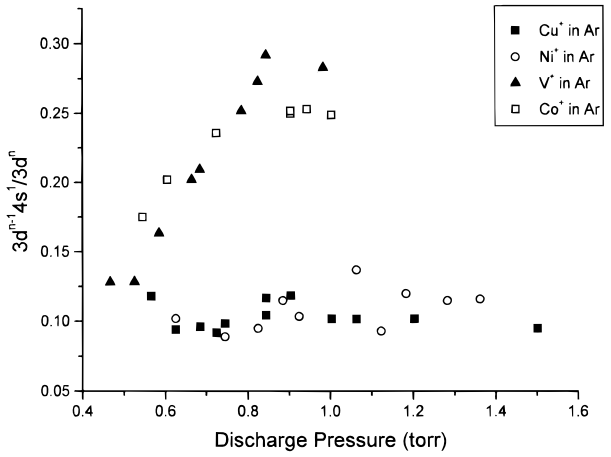

Figure 4. High-mobility/low-mobility ratios for V^+, Co^+, Ni^+ and Cu^+ as a function of discharge pressure. Discharge current = 2.6, 1.5, 3.0, 3.0 mA respectively; sampling distance = 13 mm for V^+, Ni^+, Cu^+ and 16 mm for Co^+. All ions sampled from Ar discharges.

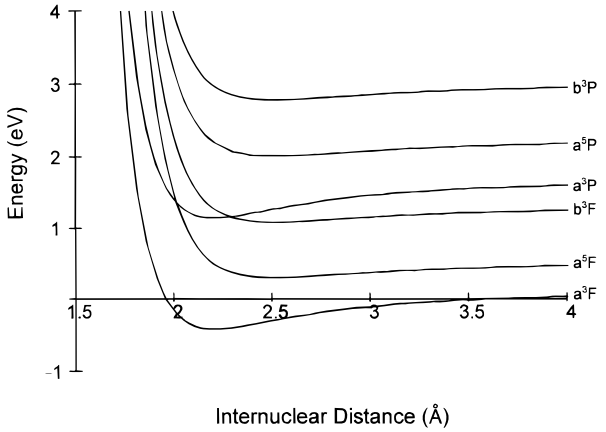

Figure 5. *n*-6-4 potential energy surfaces for low-lying Co^+ states interacting with Ar. Parameter values used: ($3d^8$) ϵ = 49.1 kJ/mol, γ = 0.34, n = 12.2; ($3d^74s^1$) ϵ = 21.0 kJ/mol, γ = 0.067, n = 12.4.

that might arise from pressure-induced changes in the plasma dimensions. For all four ions, the low-mobility configuration predominates under these conditions. Given that the lowest-lying excited state for each is a high-mobility configuration, we interpret these ratios to indicate that the ground state is in greatest abundance. However, this does not mean that excited states of the same configuration as the ground state are not present, since several states may have the same configuration. Thus, the measured $3d^{n-1}4s^1/3d^n$ ratio will reflect the total contribution to each configuration by the existing state distribution at that particular discharge pressure and/or position within the plasma.

A recent study has suggested that ions that are sampled from the GD are formed very near the sampling orifice.[15] If so and given the premise that fast electrons are required for excitation, then the configuration distribution that we observe is largely the result of the electron energy distribution function at that distance and pressure within the NG. The spatial dependence noted above is consistent with this idea; however, our observations, particularly the behavior of Co^+ and V^+, suggest that at least a portion of the sampled ions experience a number of relaxing collisions with the discharge gas prior to extraction. The data in Figure 4 would appear to contradict this relaxation argument since both Co^+ and V^+ clearly indicate an enhancement of the high-mobility configuration at higher discharge pressures, but the enhancement of the high-mobility peak may in fact be due to deactivation of one or more higher-lying low-mobility states. Examination of Table 2 reveals that for these two ions, there are low-lying states of both $3d^{n-1}4s^1$ and $3d^n$ configurations. In particular, the ordering of the excited states for both of these ions is such that interaction with the discharge gas results in curve-crossing (such as that described above for Fe^+) between excited states, resulting in enhancement of a lower-lying $3d^{n-1}4s^1$ configuration. This effect can be qualitatively modeled using a parametrized *n*-6-4 potential energy surface that has been developed previously.[20]

$$V(r) = \frac{n\epsilon}{[n(3+\gamma) - 12(1+\gamma)]} \times \left[\frac{12}{n}(1+\gamma)\left(\frac{r_m}{r}\right)^n - 4\gamma\left(\frac{r_m}{r}\right)^6 - 3(1-\gamma)\left(\frac{r_m}{r}\right)^4\right] \quad (1)$$

Potential energy curves constructed using this model are shown in Figure 5 for the Co^+/Ar system. The specific shapes of these curves depend on the three adjustable parameters, ϵ, the well-depth, n, the exponent on the repulsive component, and γ, the contribution to the attractive component by the $1/r^4$ and $1/r^6$ terms. r_m is the equilibrium distance for the interaction, which is defined in terms of the other three variables. Values for these parameters for the two Co^+ configurations in He and Ne have been previously determined by fitting temperature-dependent mobility data in each gas.[20] No data are available for metal ions in Ar since its higher polarizability results in unresolved arrival times for the two metal ion configurations. Values of ϵ, γ, and n for the two Co^+ configurations in Ar used in Figure 5 were estimated from published data for Co^+ in He and Ne. Given these estimations, these curves indicate that crossing occurs between the low-mobility a^3P state and the high-mobility a^5F and b^3F states, both of which are lower in energy. Variations of ±10% in the values of ϵ, γ, and n do not alter the fact that these curve crossings occur as long as the $3d^74s^1$ surfaces are more repulsive than the $3d^8$ surfaces. It has also been shown that spin−orbit coupling in the metal (not considered in Figure 5) should result in multiple curve crossings for the a^3P term.[20] Thus, it seems likely that efficient quenching of the a^3P state can occur prior to extraction from the discharge given sufficient numbers of collisions with the discharge gas.

Presumably, similar curves could be constructed for the V^+/Ar system; however, values for ϵ, n, and γ are not available for this metal in any gas. Nonetheless, given the ordering of the states, similar curve crossings occur. High-mobility/low-mobility configuration ratios for Cu^+ and Ni^+ do not appear to be significantly influenced by discharge pressure. Examination of Table 2 reveals that all accessible excited states for both of these ions are high-mobility configurations. As a result, these excited states are not coupled to the low-mobility ground state via curve-crossing for either ion. Inefficient collisional relaxation of isolated Ni^+ excited states has been observed in Ne[21] and should occur in Ar as well; however, complete deactivation is believed to require many (in excess of 1000) collisions.[7] The observed insensitivity of the configuration ratios of Ni^+ and Cu^+ as a function of discharge pressure suggests that few relaxing collisions occur prior to sampling.

The observed influence of interaction with the discharge gas suggests that the efficiency of an individual relaxing collision between excited metal ions and the discharge gas will also be important in defining the state distribution of the metal ion. We have previously reported that the high-mobility/low-mobility configuration ratio for Cu^+ can be increased by the addition of He to the discharge.[2] Similar effects are observed with Au^+,

Pt^+ (see below), and Ni^+. In the cases in which it has been used, Ne appears to be comparable to He in its ability to enhance formation of excited-state ions and has the added benefit of a much higher sputter yield than He.[22] Kemper has also noted that the relative amount of Ni^+ excited state produced in different rare gas discharges followed the trend He > Ne > Ar > Kr.[23] While these observations are consistent with the expected behavior based on the relaxing efficiencies of the discharge gases, it is difficult to conclude that this effect is solely the result of collisional efficiency, since the identity of the discharge gas influences the plasma conditions governing potential excitation mechanisms as well. These factors include differences in the EEDF's, as well as selective population of excited metal ion states by ions or metastables of the discharge gas.[16,24]

Third-Row Metal Ions. The behavior of third-row ions extracted from the discharge further supports the idea that some limited interaction with the discharge gas occurs that can facilitate changes in the internal state distributions of the ions when relaxation pathways are available. ESC analysis of the state distributions of sputtered third-row ions is more challenging than that with the first-row ions because the resolution of the ATD's is inherently poorer. This arises for several reasons. First, the difference in the sizes of 6s and 5d orbitals is less than that of the 4s and 3d by approximately 30%.[25,26] This results in a reduction of the differences in the mobilities of the $5d^n$ vs $5d^{n-1}6s^1$ configurations. Further, several of the third-row ions possess low-lying excited states that differ from the ground state by either the presence or absence of a second 6s electron. We have no evidence to indicate that the mobility of a $5d^{n-2}6s^2$ state is sufficiently different from that of a $5d^{n-1}6s^1$ state to be resolvable via ESC. Because of these potential difficulties, all of the third-row ATD's except for Hg^+ were acquired with the drift cell at a reduced temperature in addition to room temperature to improve chromatographic resolution. All low-temperature ESC experiments were carried out between 180 and 208 K.

One notable feature of the third-row ATD's is that all of them exhibited tailing at long arrival times at low temperature, and those of the early metals (Hf^+, Ta^+, W^+, and Re^+) exhibited tails at all temperatures. This feature does not necessarily indicate the presence of excited states, although the presence of a small amount of a low-mobility configuration could be obscured within the tail of a large high-mobility feature. Instead, we attribute tailing in these ATD's to the presence of some associated species involving the metal ion. Without exception, tailing was noted when mass spectra of the ions exiting the drift cell indicated the presence of species containing the metal ion combined with either oxygen or water or both. The effect is more pronounced with the early metals due to their propensity to form oxides, but at reduced temperatures, the late metals were also observed to participate in reactions, primarily clustering with water. Because these metal oxides and hydrates possess lower mobilities than the bare metal, they have longer residence times in the drift cell. If dissociation occurs within the drift cell, the flight time of the subsequently detected metal ion is longer than that of a "never-reacted" metal ion. Because the dissociation may occur at any point within the drift cell, a range of arrival times is observed, with the shortest being attributable to metal ions never involved in a reaction. For most metals, we observed a decrease in the amount of reaction products accompanied by an increase in the symmetry of the ATD's as the cathode was sputtered. This suggests that some portion of the observed molecular ions is produced within the discharge and diminishes as the cathode surface is sputtered.

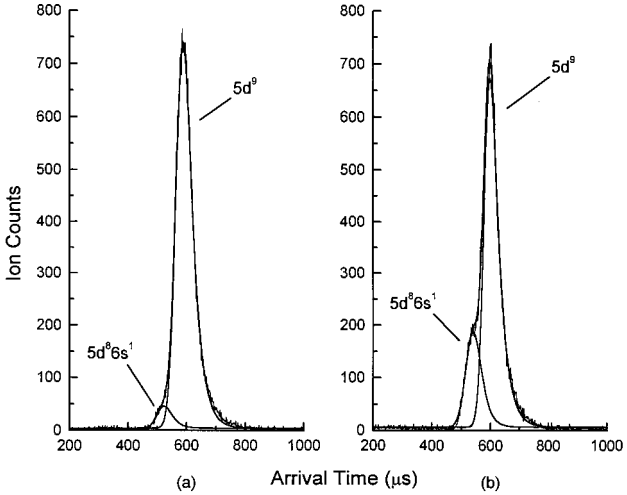

Figure 6. Arrival time distributions for Pt^+ extracted from (a) a pure Ar discharge and (b) a Ar/He discharge. $T = 186$ K; E/N=2.2 Td.

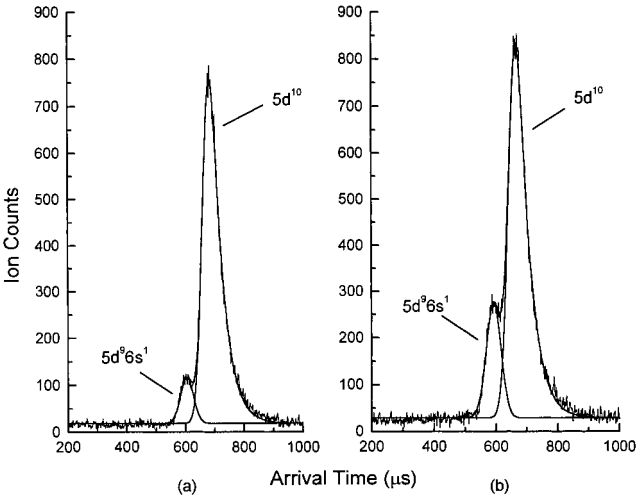

Figure 7. Arrival time distributions for Au^+ extracted from (a) a pure Ar discharge and (b) a Ar/He discharge. $T = 203$ K; E/N=2.7 Td.

Clear indications of the presence of excited configurations were observed with only two third-row ions, Pt^+ and Au^+. Partially resolved ATD's were obtained for both ions at low temperatures which show that species possessing higher mobilities than those of the ground states for these ions are being extracted from the discharge. These ATD's are shown in Figures 6 and 7. As previously noted, the relative amount of the high-mobility species for both ions increases when He is added to the discharge gas. Indeed, the enhancement of the high-mobility configuration in the He-enriched discharge was used to confirm the presence of a second peak in the less resolved Pt^+ ATD. We have assigned electron configurations of $5d^86s^1$ and $5d^96s^1$ to the high-mobility species for Pt^+ and Au^+, respectively. Estimates of the K_0 values for these high-mobility configurations based on differences in arrival times are given in Table 1. For Au^+, the only states that are energetically accessible based on our first- and second-row observations are the $^3D_3$, $^3D_2$, and $^3D_1$ states at 1.865, 2.187, and 3.442 eV above the ground-state, respectively; however, we note that the $^1D_2$ state at 3.672 eV above the ground state possesses the same configuration and would be indistinguishable from the $^3D_{3,2,1}$ states via ESC. Pt^+ has several $L-S$ terms with the appropriate configuration within the accessible energy range including ^4F, ^4P, ^2F, and the lowest J terms of the ^2D and ^2P states. The lowest J term of the $^4F(5d^76s^2)$ state is also accessible; however, as has been stated,

we do not anticipate that the increase in size arising from a doubly occupied 6s orbital will substantially alter the mobility from that of a $5d^86s^1$ configuration.

While no configuration crossings of the type described above for Fe^+, Co^+, and V^+ occur among these low-lying Pt^+ $L-S$ terms, several of these terms exhibit significant overlap of J terms due to spin−orbit coupling. If the interaction of each individual spin−orbit state with the discharge gas is considered, we see that similar "J-crossings" can occur. Specifically, if the configurations of the two J terms are such that the more attractive surface lies above the less attractive surface, then coupling between overlapping J terms must occur in the same manner as has been described for Fe^+, Co^+, and V^+. In the Pt^+ ion, crossings of this type occur between the $^2D_{3/2}$ (the upper J term of the ground state) and the $^4F_{9/2}$ term (the lowest J term of the first excited state). Depending on the specific shapes of the potential energy curves, other J terms in the ^4F manifold could be coupled to the $^2D_{3/2}$ state as well. The possibility must also be considered that the interaction with any given (non-singlet) J term with the discharge gas actually occurs on multiple curves correlating to different molecular states. This must occur in states with $5d^n$ configurations, but may also occur in $5d^{n-1}6s^1$ states as a result of the similar sizes of the 5d and 6s orbitals. This behavior is thought to give rise to efficient quenching within a given spin−orbit manifold[20] and should also facilitate quenching between overlapping $L-S$ terms in ions with large spin−orbit coupling. In Pt^+, this would result in efficient conversion of ^4F ions to the $^2D_{5/2}$ state (the lowest J term of the two interacting states). Thus, we feel that the low-mobility feature in the Pt^+ ATD is likely attributable to this state. No explicit J-crossings occur between the ^4P and ^2F terms because the configurations of these two states are both $5d^86s^1$; however, the presence of multiple curves could result in efficient relaxation within these two manifolds as well. Exactly how much or how little coupling between these two excited terms occurs is not known, yet a high-mobility ion is clearly extracted from the He-enriched discharge. This indicates that, even if the ^4P and ^2F terms are coupled to each other to some degree, one or more ^4P or ^2F spin−orbit states is isolated from lower states. We therefore conclude that the high-mobility feature we observe is some distribution of the spin−orbit terms of the ^4P and ^2F states, with possible contributions from low-lying spin−orbit terms of the higher $L-S$ states of the same or indistinguishable configuration(s).

ATD's for Hf^+, Ta^+, W^+, Re^+, and Ir^+ indicate no significant contribution by species of different mobilities. All of these ions possess excited states of sufficiently low energy such that we would expect significant population of them in the absence of efficient relaxation. Accessible excited states of both Hf^+ and Re^+ possess either the same configuration as the ground state or a configuration expected to be unresolvable from the ground state; however, Ta^+, W^+, and Ir^+ all possess excited states that should be observable based on their mobilities if present. Examination of the accessible terms for these third-row ions (see ref 10a and 10c) reveals that numerous configuration crossings and J-crossings such as those described above for Pt^+ can occur. Here also, as in the case of Pt^+, multiple interactions between J substates can further enhance conversion between spin−orbit terms and therefore between overlapping $L-S$ terms. This suggests that the majority of excited states for these ions are relaxed to either the ground state or to isolated states of the same (or indistinguishable) mobility as the ground state. In the case of Re^+, the presence of excited states unresolvable from the ground state seems likely. This ion's ground state is $^7S(5d^56s^1)$, and its first excited state is $^5D(5d^46s^2)$, for which the lowest spin−orbit term lies 1.7 eV above the ground state. Higher excited states possess the $5d^56s^1$ configuration and should be converted to the ^5D term via configuration crossing. This type of curve-crossing should not occur between the ^7S state and the ^5D state since the $5d^46s^2$ configuration should experience a less attractive interaction with the discharge gas than the $5d^56s^1$ configuration. Further, the ground state is a singlet state; therefore, the interaction of this term with the discharge gas will occur on a single curve. As a result, efficient quenching of ^5D states to the ^7S state should not occur. Thus, Re^+ represents a case where energetics suggests that the ^5D state can be populated and no efficient relaxation mechanism is apparent. Therefore, we feel that it is likely that some amount of this excited state is present in the Re^+ ions sampled from the discharge but is not resolved in the ATD.

Summary

Clearly, the sputtering glow discharge is a viable means of producing a wide variety of metal ions for use in ion−molecule reactions. This work has illustrated that this ion source produces long-lived excited metal ions in many cases. Given the sensitivity of metal ion chemistry to the electronic configuration of the ion, the possible presence of these excited ions must be accounted for if they are to be used in subsequent reactions. Ideally, it is desirable not only to quantify the state distributions of the metal ions but to establish some degree of control over them as well. The ESC experiments detailed here indicate that excited metal ion configurations within approximately 3.4 eV of the ion ground state can be populated in Ar, Ne, and He discharges. Further, the mechanism by which excited ions are formed appears to involve fast electrons entering the negative glow after being accelerated across the cathode fall. This excitation mechanism produces a distribution of states that can be subsequently influenced by collision in some cases. Evidence suggests that collisional deactivation is a factor in ions where crossings occur between the potential energy surfaces describing the interaction of the different ion electronic states with the discharge gas. This idea is further supported by the observation that collisional deactivation within the discharge appears to be enhanced in heavy ions where large spin−orbit coupling results in numerous such curve crossings. The influence of collisions with the discharge gas is not as pronounced for ions (such as Cu^+ and Ni^+) in which different electronic states are not coupled in this way. Taken together with the observed spatial effects, this indicates that extracted metal ions are formed very near the sampling orifice and excited state populations are therefore enhanced by sampling nearer the cathode. Other factors that enhance excited state populations include lower discharge pressures and for some ions, a working gas composition that relaxes the excited states less efficiently. Thus, while it does not appear that "discharge recipes" exist that would selectively produce a specific excited state, it is clear that some degree of manipulation of the internal state distributions is possible, thus enhancing the utility of the glow discharge in examinations of metal ion chemistry.

Acknowledgment. This work was supported in part by a Cottrell College Science Award of Research Corporation. Acknowledgment is also made to the donors of the Petroleum Research Fund, administered by the ACS, for partial support of this research.

References and Notes

(1) *Glow Discharge Spectroscopies*; Marcus, R. K., Ed.; Plenum: New York, 1993.

(2) Taylor, W. S.; Campbell, A. S.; Barnas, D. F.; Babcock, L. M.; Linder, C. B. *J. Phys. Chem. A* **1997**, *101*, 2654−2661.
(3) Taylor, W. S.; Everett, W. R.; Babcock, L. M.; McNeal T. L. *Int. J. Mass Spectrom. Ion Proc.* **1993**, *125*, 45−54.
(4) Tjelta, B. L.; Armentrout, P. B. *J. Am. Chem. Soc.* **1996**, *118*, 9652−9660.
(5) Armentrout, P. B. *Annu. Rev. Phys. Chem.* **1990**, *41*, 313−344.
(6) Weisshaar, J. C. in *Advances in Chemical Physics*; Ng, C. Y., Baer, M., Eds.; Wiley and Sons Inc.: New York, 1992; Vol. 82.
(7) van Koppen, P. A. M.; Kemper, P. R.; Bowers, M. T. in *Organometallic Ion Chemistry*; Freiser, B. S., Ed.; Kluwer Academic Publishers: Boston, 1996.
(8) Kemper, P. R.; Bowers, M. T. *J. Phys. Chem.* **1991**, *95*, 5134−5146.
(9) Lindinger, W.; Albritton, D. L. *J. Chem. Phys.* **1975**, *62*, 3517−3522.
(10) (a) Moore, C. E. *Atomic Energy Levels*; U.S. National Bureau of Standards: Washington, DC, 1952; Circ. 467 (U.S. Natl. Bur. Stand.). (b) Sugar, J.; Corliss, C. *J. Phys. Chem. Ref. Data* **1981**, *10*, 197−289; **1981**, *10*, 1097−1174; **1992**, *11*, 135−241; **1990**, *19*, 527−616. (c) van Kleef. Th. A. M.; Metsch, B. C. *Physica* **1978**, *95C*, 251−265.
(11) Loh, S. K.; Fisher, E. R.; Lian, Li; Schultz, R. H.; Armentrout, P. B. *J. Phys. Chem.* **1989**, *93*, 3159−3167.
(12) Hess, K. R.; Harrison, W. W. *Anal. Chem.* **1988**, *60*, 691−696.
(13) Smith, R. L.; Serxner, D.; Hess, K. R. *Anal. Chem.* **1989**, *61*, 1103−1108.
(14) Bogaerts, A.; Gijbels, R.; Goedheer, W. J. *Anal. Chem.* **1996**, *68*, 2296−2303.
(15) Hang, W.; Harrison, W. W. *Anal. Chem.* **1997**, *69*, 4957−4963.
(16) Steers, E. B. M.; Fielding, R. J. *J. Anal. At. Spectrom.* **1987**, *2*, 239−244.
(17) Fang, D.; Marcus, R. K. *Spectrochim. Acta* **1991**, *46B*, 983.
(18) Steers, E. B. M.; Leis, F. *J. Anal. At. Spectrom.* **1989**, *4*, 199−204.
(19) Bogaerts, A.; Gijbels, R. *Anal. Chem.* **1996**, *68*, 2676−2685.
(20) von Helden, G.; Kemper, P. R.; Hsu, M.; Bowers, M. T. *J. Chem. Phys.* **1992**, *96*, 6591−6605.
(21) Kemper, P. R.; Hsu, M.; Bowers, M. T. *J. Phys. Chem.* **1991**, *95*, 10600−10609.
(22) Harrison, W. W.; Bentz, B. L. *Prog. Anal. Spectrosc.* **1988**, *11*, 53−110.
(23) Kemper, P. R.; Weis, P. Personal communication.
(24) Wagatsuma, K.; Hirowaka, K. *Anal. Chem.* **1988**, *60*, 702−705.
(25) Irikura, K. K.; Beauchamp, J. L. *J. Phys. Chem.* **1991**, *95*, 8344−8351.
(26) Barnes, L. A.; Rosi, M.; Bauschlicher, C. W. *J. Chem. Phys.* **1990**, *93*, 609−624.